Materials Chemistry and Physics 258 (2021) 123978

Contents lists available at ScienceDirect

Materials Chemistry and Physics

journal homepage: www.elsevier.com/locate/matchemphys

Cell viability and collagen deposition on hydroxyapatite coatings formed on pretreated substrates

A. Yanovska [a,*], Ye Husak [a], O. Mishchenko [b], A. Gudakov [c], O. Oleshko [a], A. Yusupova [a], M. Vielikov [d], J. Radwan-Pragłowska [e], M. Piątkowski [e], Ł. Janus [e], E. Szajna [b], M. Pogorielov [a,b]

[a] Sumy State University, 2, Rymskogo-Korsakova Str, Sumy, 40007, Ukraine
[b] NanoPrime, Metalowcow 23, Debica, 39-200, Poland
[c] Institute of Applied Physics, NAS of Ukraine, 56, Petropavlivska Str, Sumy, 40000, Ukraine
[d] MU-Pleven, 1, Saint Kliment Ohridski Str, Pleven, 5800, Bulgaria
[e] Faculty of Chemical Engineering and Technology, Cracow University of Technology, Warszawska 24 Str, 31-155, Poland

HIGHLIGHTS

- Various surface pretreatments for sandblasted Ti-6Al-4V substrates has been investigated.
- Three types of pretreatments: by 20% NaOH, 20% oxalic acid and their mixture was applied.
- Hydroxyapatite (HA) coatings were obtained by thermal deposition technique.
- Obtained coatings showed osteoblastic cell adhesion in 1 day of the experiment.
- HA coatings makes substrates more osteoconductive due to increasing of collagen synthesis.

GRAPHICAL ABSTRACT

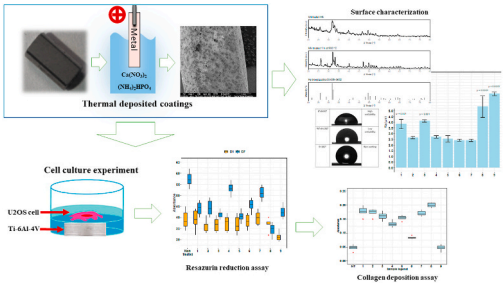

ARTICLE INFO

Keywords:
Thermal deposition
Hydroxyapatite coatings
Chemical pre-treatment
Collagen production

ABSTRACT

A method of thermal deposition that involves localized high peak temperatures at the electrode-electrolyte interface was proposed for hydroxyapatite (HA) coatings deposition. Active surface layers were obtained by HA incorporation from the aqueous electrolyte into the substrate surface due to the decrease of HA solubility with increasing of substrate temperature. Commercially Ti-6Al-4V alloy (grade 4) substrates were pretreated by sandblasting combined with various chemical pre-treatments: 20% NaOH, 20% oxalic acid, and both. After both types of pre-treatment and HA thermal deposition, we can observe uniform coatings with a rough surface. HA presence was confirmed by X-ray Diffraction (XRD) and Fourier-transform infrared spectroscopy (FTIR) analysis. According to received data, samples after 6.5 bar, one cycle of sandblasting and etching in 20% oxalic acid 2 h, 20% H_3PO_4 1 min as well as untreated samples showed the highest wettability. All measured contact angles are lower than 90°, which means that obtained HA surfaces are hydrophilic and indicates that the wetting of the surface is favorable, and the fluid will spread over a large area of the surface.

Resazurin reduction assay showed satisfactory U2OS osteoblastic cell adhesion in 1 day of the experiment. There is no significant difference between non-treated polished surfaces and HA-covered with sandblasting pre-treatment. In contrast – the polished surface with HA coating demonstrates significantly less cell adhesion.

* Corresponding author. Sumy State University, Theoretical and Applied Chemistry Department, 2, Rymskogo-Korsakova Str, Sumy, 40007, Ukraine.
E-mail address: yanovskaanna@gmail.com (A. Yanovska).

https://doi.org/10.1016/j.matchemphys.2020.123978
Received 18 July 2020; Received in revised form 21 September 2020; Accepted 22 October 2020
Available online 24 October 2020
0254-0584/

It was confirmed low collagen production both in untreated and polished-HA surfaces in comparison with the sandblasted-HA ones. The obtained data suggest that roughness plays an important role in cell adhesion and proliferation, but HA coating provides additional stimuli for cell activity (collagen synthesis).

1. Introduction

Ti-6Al-4V alloy is a widely used implant material due to its biocompatibility and excellent mechanical properties [1]. However, the release of metal ions in the physiological environment and lack of osteoconductivity is still a big problem [2]. Therefore, the implant surface should be treated for increased corrosion resistance and bioactivity by calcium phosphate coatings formation [3]. Hydroxyapatite $Ca_{10}(PO_4)_6(OH)_2$ is the main mineral component of bone tissue [4], and clinical studies proved that HA-coated hip implants show exceptionally high survival rates exceeding 95% at ten years observation time [5,6]. HA-coated dental implants showed survival rates between 79 and 96% at eight years of observation time [7]. Various kinds of techniques should be applied to obtain hydroxyapatite coatings [8–15]. Among them are sol-gel [8], magnetron sputtering [9], pulsed laser deposition [10], electrophoretic deposition [11], electrochemical deposition [12], plasma spray [13,14]. Some of these methods provide coatings with weak adhesion to the metallic substrates, cracks, the necessity of great sintering temperatures, long processing time, degradation during long-term implantation, and high cost [15]. Plasma Electrolytic Oxidation (PEO) is a promising technique for obtaining active surface layers [16–18] on metal substrates and alloys with complex geometries. Using PEO, the corrosion-resistant, porous, and bioactive substrates with hydrophilic surfaces were obtained. It is an advanced electrochemical technique based on anodizing at high voltages in aqueous electrolyte solutions. It consists of numerous simultaneous plasma discharges, leading to localized high temperature and high pressure at the metal surface [3,16–20]. In our work, we propose a method of thermal deposition that also belongs to low-temperature deposition techniques, that is carried out at temperatures much below the incongruent melting point of hydroxyapatite at 1570 °C, and involves localized high peak temperatures at the electrode-electrolyte interface. The decreasing of hydroxyapatite solubility with increasing temperature is the main principle of this method. Hydroxyapatite coatings were obtained after the passing of current from solutions containing Ca^{2+} and PO_4^{3-} ions by increasing the substrate temperature [21]. An active surface layer can be obtained by HA incorporation from the electrolyte into the substrate surface. For this purpose, we used as prepared suspension of hydroxyapatite nanoparticles. The ways of substrate pre-treatment influenced coating surface formation [22], so in our work, we propose a comparison of various surface pre-treatment and estimation of their impact on coatings formation.

In this work, we propose HA coatings deposition onto commercially Ti-6Al-4V alloy samples (Grade 4), that were pretreated by different ways in an aqueous electrolyte containing a suspension of nano dispersed hydroxyapatite. Post-treatment of obtained coatings by Laser-Induced Periodic Surface Structures (LIPSS) will be reported in our future works.

2. Materials and methods

2.1. Hydroxyapatite synthesis

Synthesis of stoichiometric hydroxyapatite was provided by the following reaction:

$$10Ca(NO_3)_2{\cdot}4H_2O + 6(NH_4)_2HPO_4 + 8\ NH_3{\cdot}H_2O \rightarrow Ca_{10}(PO_4)_6(OH)_2 + 20NH_4NO_3 + 46H_2O$$

Two different solutions were prepared separately:

Solution 1.

0.1 M $Ca(NO_3)_2$ solution was prepared by dissolving an appropriate amount of $Ca(NO_3)_2{\cdot}4H_2O$ in distilled water. The solution was heated under stirring up to 75 °C. Then 25% ammonia solution was added dropwise to the calcium nitrate solution to get basic pH (pH = 12).

Solution 2.

0.06 M $(NH_4)_2HPO_4$ solution was prepared. Then, the second solution was added dropwise to the first solution for obtaining hydroxyapatite under stirring and heating up to 80 °C for 2 h. After 2 h, the pH was decreased to 9. The top solution was removed by decantation. After that, the precipitate was washed three times until pH ≈ 7 was obtained. After decantation as-prepared solution with HA slurry was used for thermal deposition treatment of samples.

2.1.1. Hydroxyapatite coatings deposition

Ti-6Al-4V samples (grade 4) with size 4.2 × 3.48 × 7.98 mm were used as the substrates for the thermal treatment. The specimens for thermal deposited coatings (TDC) were pretreated with sandblasting to obtain a rough surface with pressure 4.5 and 6.5 bar 1 or 2 cycles of sandblasting treatment (Table 1). After sandblasting, two types of etching were applied: in 20% oxalic acid, in 20% NaOH, or sequentially in both. Finally, all samples were treated in 20% H_3PO_4 for 1 min. For the control group, the same samples without sandblasting pre-treatment were prepared by washing them thoroughly with distilled water followed by washing in ethyl alcohol (Table 1, sample 9).

The thermal deposition process was carried out using an electrochemical unit with cathode and anode with the cooling system provided by Nanoprime (Poland) and equipped with a pulsed bipolar DC power supply Solvix Power Supply RS/RS-485 with Solvix control software (Solvix GmbH. Switzerland). The temperature of the electrolyte was kept below 25 °C using a cooling system. The frequency was the same for all experiments – 100 kHz.

A titanium chamber containing the electrolyte used as a cathode, and the titanium substrate, immersed in the electrolyte used as an anode.

Table 1
Samples preparation and experimental conditions.

Sample number	Surface pre-treatment	Deposition parameters		
		U, V Given/ Real	I, A Given/ Real	Time, sec
1	Sandblasting, 6.5 b, 2p, 20% NaOH 3 h, 20% H_3PO_4 1 min	350/ 180	6/6.13	60
2	Sandblasting, 6.5 b, 1p, 20% NaOH 3 h, 20% H_3PO_4 1 min	350/ 173	6/6.13	30
3	Sandblasting, 6.5 b, 1p, 20% oxalic acid 2 h, 20% H_3PO_4 1 min	350/ 172	6/6.1	60
4	Sandblasting, 6.5 b, 2p, 20% oxalic acid 4 h, 20% H_3PO_4 1 min	350/ 180	6/6.12	30
5	Sandblasting, 4.5 b, 2p, 20% oxalic acid 4 h, 20% NaOH 1 h, 20% H_3PO_4 1 min	350/ 240	6/6.28	30
6	Sandblasting, 6.5 b, 1p, 20% oxalic acid 3 h, 20% H_3PO_4 1 min	350/ 280	6/5.30	30
7	Sandblasting, 4.5 b, 1p, 20% oxalic acid 3 h, 20% H_3PO_4 1 min	350/ 283	6/5.90	30
8	Sandblasting, 4.5 b, 1p, 20% oxalic acid 4 h, 20% H_3PO_4 1 min	350/ 258	6/6.06	30
9	Without pretreatment	350/ 247	6/2.02	30

The electrolyte bath during the process was water-cooled to maintain the bath temperature close to room temperature. The electrolyte solution was kept under continuous stirring during the process by a magnetic stirrer to ensure uniform electrolyte concentration and dissipation of the heat generated. After the treatment, the samples were cleaned with distilled water and air-dried at room temperature.

2.2. Materials characterization

2.2.1. Characterization techniques

The morphology analysis of obtained composites was provided by scanning electron microscopy (SEO-SEM Inspect S50-B) with energy dispersive spectrometer AZtecOne with detector X-MaxN20 (Oxford Instruments plc.). The X-ray diffraction (XRD) analysis was carried out by the X-ray diffractometer DRON-3M (Bourevestnik, www.bourevestnik.ru) connected to a computer-aided system for experiment control and data processing. The CuKα radiation was used (wavelength 0,154 nm) with the Bragg-Brentano focusing method. The current and the voltage of the X-ray tube were 20 mA and 40 kV, respectively. The scan performed in a continuous registration mode with a 0.02° step and 1°/min scan speed in 2 θ range of 10° – 60°. All experimental data were processed using the DifWin-1 program package (Etalon-TC, www.specord.ru). Phase identification performed using the JCPDS (Joint Committee on Powder Diffraction Standards) card catalog.

Molecule structural components were identified by Fourier Transform Infrared Spectroscopy method using ThermoNicolet Nexus 470 apparatus purchased from Thermo Fisher Scientific (Waltham, MA, USA) equipped with ATR adapter. Measurements and analysis of spectra were carried out with the use of software attached to the device. The spectra were recorded in the spectral range of 550–4000 cm^{-1} with a nominal resolution of 4 cm^{-1} and 32 scans for each measurement. All samples were dried before the analysis.

2.2.2. Wettability and contact angle measurement

The static contact angle provides valuable information about the properties of the surface. The contact angle is frequently used to characterize the wettability of the surface. The static contact angle gives valuable information about the hydrophobicity properties of the surface. Contact angle (CA) measurements experiments were made using a video-based optical contact angle measuring instrument (OCA 15 EC, Series GM-10-473 V-5.0, Data Physics, Filderstadt, Germany). Ultrapure water droplets of about 0.5 μL were dropped onto the solid surface of the samples through a syringe at room temperature. CA was calculated with the aid of an illumination system and software [23]. At least five different positions of each surface were measured, and the average value was noted. The optical analysis of drops that hang from a dosing needle or are placed on a solid surface facilitates the determination of different surface and interfacial parameters. The contact angle that a liquid drop establishes on a solid surface characterizes the solid's wetting behaviour with a given liquid.

So, the wettability of the Ti rods was quantified by the sessile drop technique. The angles between the tangent of the drop at the solid/liquid/gas tree phase boundary and the horizontal baseline of the solid surface were obtained. CA (θ) characterizes the hydrophilicity of the surface when the water has been used as a wetting agent [24]. Water contact angles lower than 90° designate surface as hydrophilic and indicates that wetting of the surface is favorable, and the fluid will spread over a large area of the surface, while surfaces with water contact angle above 90° are considered hydrophobic and generally means that wetting of the surface is unfavorable [25]. The CA data was recorded for ultra-pure water, for at least three parallel samples.

2.2.3. Roughness measurement

Surface roughness is a quantitative value of the geometric contour of a surface. It was determined by the tactile stylus method in which a 2-dimensional profile is measured mechanically by scanning a cantilever tip over a surface [26]. Roughness characteristics were obtained over 10 mm, using a surface roughness tester (Surftest SJ-301, Mitutoyo, Kawasaki, Kanagawa, Japan). According to the EN ISO 4287:1999 [27] and DIN 4768 [28] standards, the following roughness parameters were examined: arithmetic means of the sum of roughness profile values (Ra), mean peak-to-valley height (Rz).

2.2.4. Cell culture experiments

The cells (U2OS cell type) were grown in 75 cm^2 cell culture flasks under standard culture conditions of humidified air containing 5% CO_2 at temperature 37 °C with medium renewal every 2–3 d [29]. Dulbecco's modified Eagle medium/nutrient mixture F-12 (DMEM/F-12) with L-glutamine was used, containing 100 units mL^{-1} penicillin, 100 μg mL^{-1} streptomycin, 2.5 μg mL^{-1} amphotericin B, and 10% fetal bovine serum. Before cell seeding, all samples were sterilized in an autoclave; each sample was placed in a separate well of a 24-well cell culture plate and immersed in DMEM overnight. On the next day, the medium was removed, and U2OS cells were seeded on each sample and in the wells with non-treated samples (as negative control) at a cell density of 10^4 cells per well. Cell adhesion at 24 h and cell proliferation on samples were assessed by the Alamar blue colorimetric assay, which is used to measure cell viability. Alamar blue (Invitrogen) was added in an amount equal to 10% of the medium volume to each well. As a negative control, Alamar blue solution was added to the wells containing only a culture medium without cells. As a positive control, Alamar blue solution was added to the wells that contained only cells without samples (TCP control). The plates were incubated for 8 h at 37 °C in the dark. The medium was then transferred to another 96-well plate, and the absorbance was measured using a Multiskan FC (Thermo Fisher Scientific, Waltham, MA, USA) plate reader at wavelengths of 570 and 595 nm. The cells were quantified at different time intervals: 1 and 7 d. All experiments were repeated three times.

2.2.5. Collagen production assay

Collagen synthesized by U2OS cells and accumulated on samples was detected through staining with Sirius Red dye. The staining was performed as follows: on the 14th and 21st days of incubation, samples were transferred to other 24-well plates and washed three times with ice-cold PBS (4 °C). Then 1.5 mL of Bouin's solution was added to each well for 1 h at room temperature. After the solution was removed, samples were rinsed with cold tap water and dried in the fume hood overnight. On the next day, 1.5 mL of Sirius Red dye was added to samples for 1 h, then removed, and each well was washed four times with 0.01 M HCl. 1 mL of 0.1 M NaOH solution was added to each well in order to recover the bound dye. The plate was placed on the shaker for 30 min. After that, 100 μL of eluted dye from each well was transferred to a 96-well plate, and the absorbance was measured using Multiskan FC (Thermo Fisher Scientific, Waltham, MA, USA) plate reader at a wavelength of 550 nm.

2.3. Results and discussion

Fig. 1 Shows the FT-IR spectra of hydroxyapatite, used for thermal coating deposition.

The absorption peaks located at 1092 and 1033 cm^{-1} originated from asymmetrical stretching ($\nu 3$) of PO_4^{3-} and at 566, and 603 cm^{-1} were attributed to bending modes ($\nu 4$) of PO_4^{3-}, respectively. The symmetric stretching modes ($\nu 1$ and $\nu 2$) of PO_4^{3-} were also observed at around 961 cm^{-1}, while a weak sharp peak at 3573 cm^{-1} corresponded to the stretching vibration of the lattice OH^- ions [30,31].

The typical bands of HA that can be assigned to the PO_4^{3-} asymmetrical stretching located at the vibrational frequency of 1021 cm^{-1} ($\nu 3$), 599-561 cm^{-1} ($\nu 4$), and O−H stretching vibration at 3374 cm^{-1}, were found in an obtained sample of hydroxyapatite.

Results of XRD analysis (Fig. 2.) show that the obtained sample corresponds to hydroxyapatite (JCPDS 9-0432). For pre-treatment, the

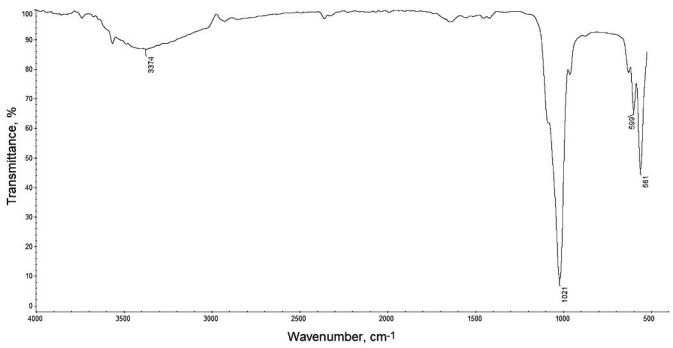

Fig. 1. FT-IR-spectrum of HA used for deposition.

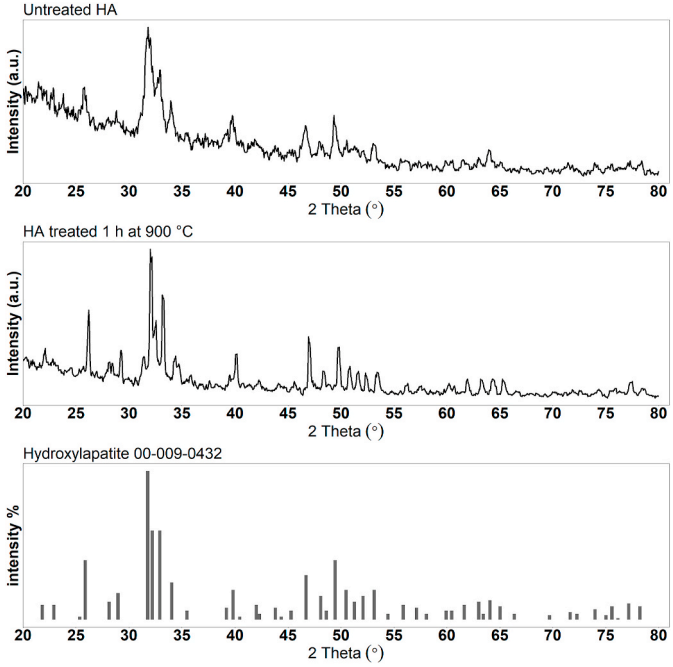

Fig. 2. XRD of as prepared and sintered at 900 °C HA powder.

as-prepared hydroxyapatite was used in the form of suspension. Sintering at 900 °C was used during the XRD investigation of powder to check the presence of β-tricalcium phosphate (β-TCP). The absence of the β-TCP phase shows that the obtained hydroxyapatite was stoichiometric. Lattice parameters of obtained samples are presented in Table 2.

Table 2
Lattice parameters (a and c) and Xs of as prepared HA compared with sintered at 900 °C and standard JCPDS card.

hkl (°)	JCPDS	As prepared HA	Treated at 900 °C HA
0 0 2	25.88	26.00	26.15
2 1 0	28.97	29.25	29.20
2 1 1	31.77	31.90	32.05
1 1 2	32.20	33.05	32.45
3 0 0	32.90	–	33.20
2 0 2	34.05	34.15	34.35
3 1 0	39.82	39.85	40.10
2 2 2	46.72	46.75	47.00
3 1 2	48.10	49.55	48.35
2 1 3	49.47	–	49.75
3 2 1	50.49	–	50.75
4 1 0	51.29	53.25	51.55
4 0 2	52.10	–	52.35
0 0 4	53.15	–	–

HA peaks in (0 0 2), (2 1 1) and (2 0 2) plane that present in diffractograms of sintered and as prepared samples, other corresponding planes for HA as identified by the JCPDS standard including (1 1 2), (3 1 2), (2 1 3), (3 2 1), (4 1 0), (4 0 2) is close for that were obtained for samples sintered at 900 °C for 1 h. Other phases except hydroxyapatite are not observed, both in as prepared and sintered samples.

Chemical pre-treatment of Ti (Grade 4) doesn't influence on the phase composition of the hydroxyapatite layer. In acidic pre-treatment, two types of etching were applied: in 20% oxalic acid, in 20% NaOH, or sequentially in both after sandblasting. Finally, all samples were treated in 20% H_3PO_4 for 1 min. Acidic etching makes the surface rougher and removes everything after sandblasting. Additional pre-treatment by 20% NaOH induced deposition of HA on the pretreated surface, but it doesn't influence phase composition (HA phase), because it was completely formed before thermal deposition.

Morphology of obtained by thermal deposition hydroxyapatite coatings are presented in Fig. 3. In all cases, we can observe uniform coatings with a rough surface. Surface pre-treatment has a great influence on obtained coatings. The morphology of the surface demonstrates an irregular and rough structure with numerous small holes observed under high magnification (× 2000). Furthermore, small micro pits and sharp edges are observed. Characteristic dimensions patterns are presented in Table 3.

These morphological surface characteristics did not change after HA coating deposition.

The HA coatings are an irregular agglomerates shape for all samples, besides 6 and 7, which were covered with uniform HA layer. The HA crystals were filled out the holes and pits. Sample without treatment has nonuniform HA layer.

Three different variants of pre-treatments were chosen: 20% NaOH (samples 1, 2), 20% oxalic acid (samples 3, 4, 6, 7, 8) and combination of pre-treatment 20% oxalic acid 4 h, 20% NaOH 1 h (sample 5) (Fig. 4).

Sample 1 and 2 were pretreated with 20% NaOH solution for 3 h and differs only by two cycles of sandblasting (sample 1) and decreased time of hydroxyapatite deposition (sample 2). Samples 3 and 4 have the same pre-treatment but differ by two cycles of pre-treatment for sample 4, power and deposition time (Fig. 3). Samples 3 and 6 differ by time of pre-treatment by 20% oxalic acid, power, and deposition time. Samples 2 and 4 differ by the type of pre-treatment by 20% NaOH (for sample 2) and 20% oxalic acid (for sample 4). Sample 5 has both types of pre-treatment by 20% NaOH and by 20% oxalic acid. Samples 6 and 7 have the same conditions but differ by the pressure of sandblasting. Samples 7 and 8 have the same conditions but differ by the time of soaking in 20% oxalic acid. Sample 9 is HA coating deposited on the untreated surface.

All obtained by thermal deposition hydroxyapatite coatings have uniform surfaces. The most uniform surface was obtained for sample 6.

Results of Roughness and Wettability measurements are given in Table 4.

The results showed a statistically significant difference between the roughness value among obtained HA coatings. The surface roughness (Table 4) displays line profile information obtained by using the tactile stylus method, respectively, for HA coatings. It should be noted that the deposited HA layer significantly increases ($P < 0.0001$) the surface roughness in the case of 8 and 9 HA samples to 5.37 and 6.51 μm while there is the resembling value in the case of the 2, 4, 5, 6, 7 HA coatings. The similarity in surface roughness of the following coatings (Ra) 2.4–2.7 μm are not statistically different (Table 4). The corresponding roughness measurements are given in Fig. 5. It was also noted for the Hydroxyapatite coatings deposition resulted in an increase in the average Ra values for the 1 and 3 HA coatings from 3.86 to 4.13 μm ($P < 0.001$). HA-coated samples 3 and 8 were obtained by thermal deposition method on the sandblasted surface by pre-treatment with 20% oxalic acid. The increase of roughness values after such type of pre-treatment could be explained by thoroughly washing and etching of sandblasted surface (sample 8 was pretreated for 4 h). The obtained surface was

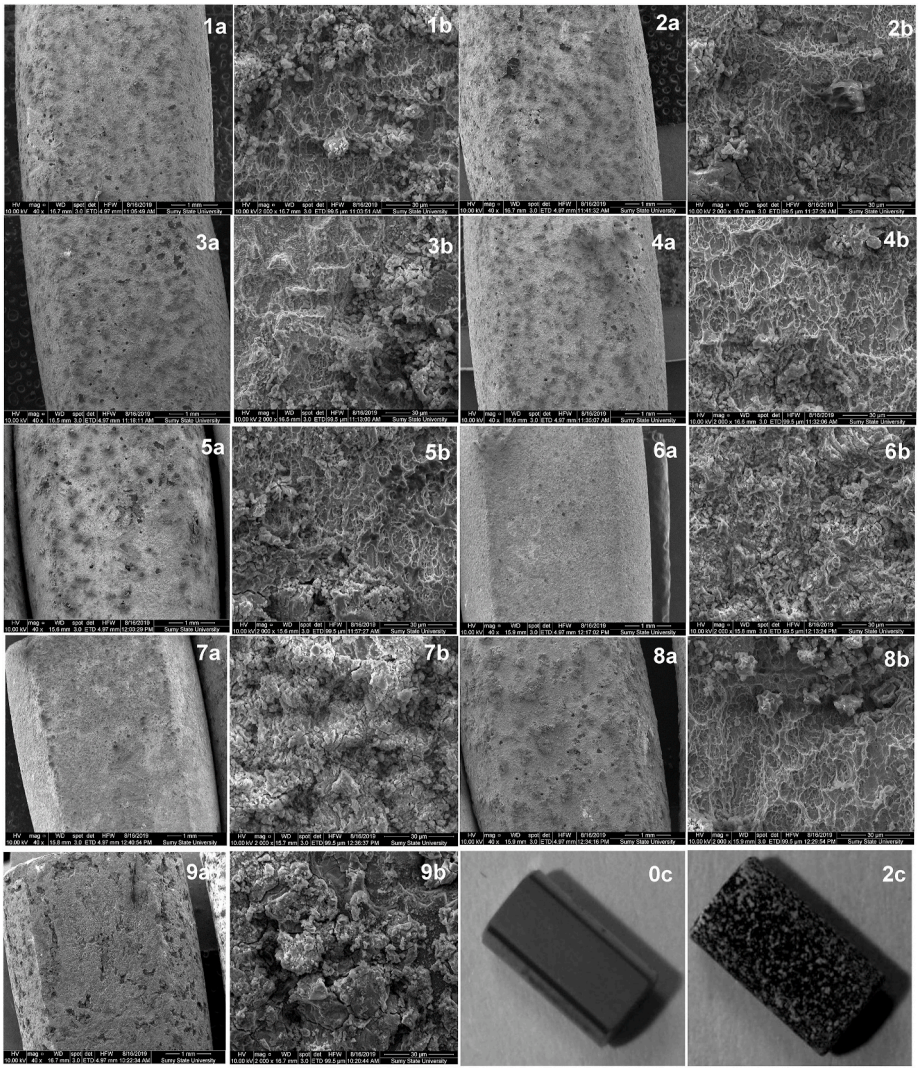

Fig. 3. Morphology of obtained calcium phosphate coatings samples 1-9 at a) x40 and b) x2000 c) general view. Sample 0 c is a sample without any treatment, and 2 c is a sample 2 general view. As well as a general view for all HA-coated samples is nearly the same, only one photo was provided.

Table 3
HA particle sizes and their distribution on the surface.

Sample number	Surface structure (holes, pits) μm^2				HA agglomerates, mm^2				N agglomerates/mm^2
	Mean	SD	Min	Max	Mean	SD	Min	Max	
1	4.82	6.76	0.22	39.61	0.0304	0.0161	0.0051	0.0682	11.11
2	5.03	6.16	0.38	29.96	0.0141	0.0066	0.0011	0.0361	11.56
3	24.116	25.73	0.19	78.29	0.0282	0.0189	0.0045	0.1039	8.39
4	18.26	20.019	0.19	78.29	0.0190	0.0120	0.0047	0.0835	10.00
5	10.75	12.67	0.49	58.12	0.0218	0.0124	0.0053	0.0620	5.89
6	19.29	19.23	0.2	79.31	Full covered, uniform layer				
7	13.18	13.67	0.50	55.13	Full covered, uniform layer				
8	15.66	16.25	0.48	82.49	0.0428	0.0488	0.0026	0.2123	5.30
9	Without treatment				Full covered, nonuniform layer				

rough, and after pre-treatment, HA coatings also have rough surfaces.

The Ra values of 2 and 4-7 samples have similar surface profile values, which are relatively lower than those in samples 1 and 3 (Fig. 5). Samples 2 and 4-7 were compared with sample 8, that shown increased surface roughness (Fig. 5). However, among all samples, the untreated surface showed higher Ra and Rz values. It can be explained by the nonhomogeneous distribution of HA on the flat surface, while on sandblasted samples, HA nanoparticles are incorporated into pores, so the obtained surface gets rough.

The contact angle measured for the control sample 9 was 22.97°, as it is shown in Table 4. The contact angle values of other coatings were 0°, except sample 3 (56.62°), for which the surface has complete wetting. According to received data, samples 3 and 9 showed the highest wettability. All measured contact angles are lower than 90°, which means that obtained HA surfaces are hydrophilic and indicates that the wetting of the surface is favorable, and the fluid will spread over a large area of the surface. The hydrophilicity of obtained coatings made them suitable for biomedical applications in dentistry.

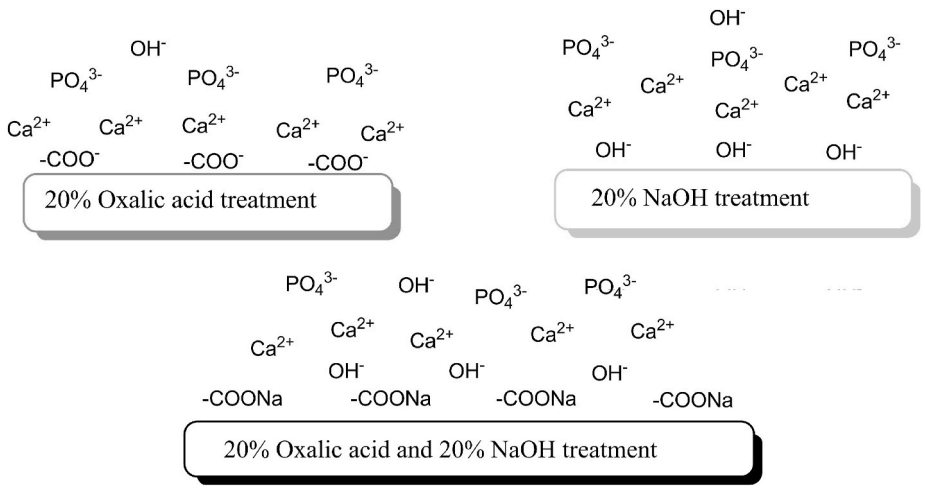

Fig. 4. Surface pre-treatment of sandblasted samples by acid, base, or their mixture.

Table 4
Characteristics of roughness and wettability of obtained coatings.

Sample number	Roughness, μm		Wettability
	Ra[1]	Rz[2]	
1	3.86 ± 0.41	22.38 ± 2.21	0°
2	2.63 ± 0.1	17.48 ± 1.35	0°
3	4.13 ± 0.1	27.7 ± 2.33	56.62°
4	2.7 ± 0.1	18.61 ± 0.88	0°
5	2.54 ± 0.28	15.82 ± 2.42	0°
6	2.43 ± 0.09	15.58 ± 0.37	0°
7	2.4 ± 0.1	15.87 ± 0.98	0°
8	5.37 ± 0.94	37.16 ± 4.73	0°
9	6.51 ± 0.15	40.66 ± 3.79	22.97°

Where: [1]Ra: the arithmetical mean of the sums of all profile values.
[2]Rz: the mean value of the total measured length.

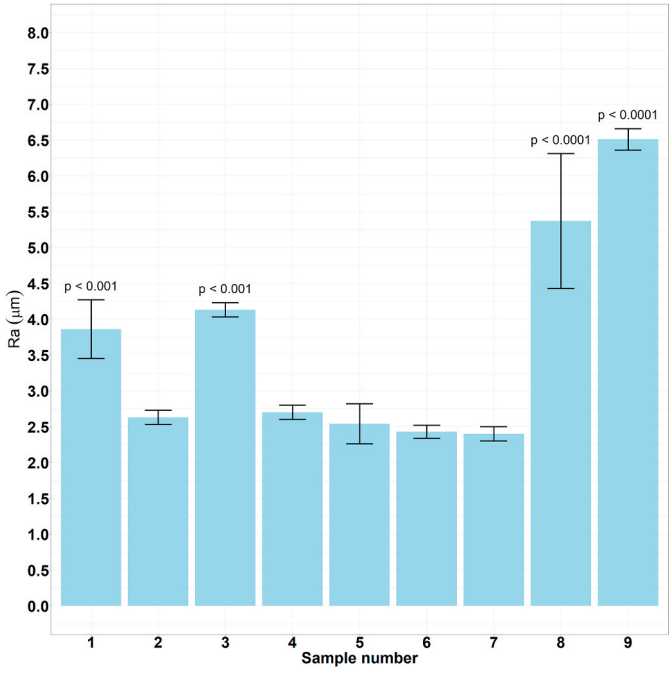

Fig. 5. Surface roughness (Ra) of HA coatings obtained by a thermal deposition method.

2.3.1. Cell culture

Resazurin reduction assay showed satisfactory U2OS osteoblastic cell adhesion in 1 day of the experiment (Fig. 6). There is no significant difference between non-treated polished surfaces and HA-covered with sandblasting pre-treatment. In contrast – the polished surface with HA coating demonstrates significantly less cell adhesion. It is known that conventional treatment did not provide sufficient HA adhesion on the metallic substrate that can be the main factor for pure cell distribution in our experiment. In 7 days, we confirm U2OS cell proliferation on polished Ti substrate and in most HA-coated ones with no significant difference between groups, but sample #5 and #8 demonstrate significantly less proliferation, probably due to unfavorable surface structure or chemical patterns. It should be noted that we have significant growth in resazurin redaction on sample 9 (with no pre-treatment) but with significantly fewer activities compare to the polished ones.

To check the hypothesis about the difference between D1 and D7, ANOVA was used (Fig. 7). Calculations made by R. Normality was

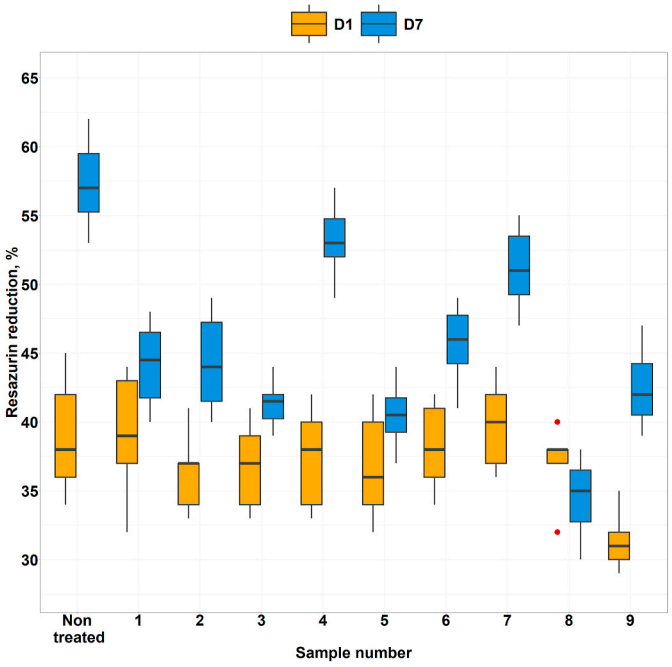

Fig. 6. Resazurin reduction assay with U2OS cells in 1 and 7 days after seeding. Statistical significance was evaluated in comparison to the non-treated (polished) Ti sample (p values after by two-tailed two samples equal variance test).

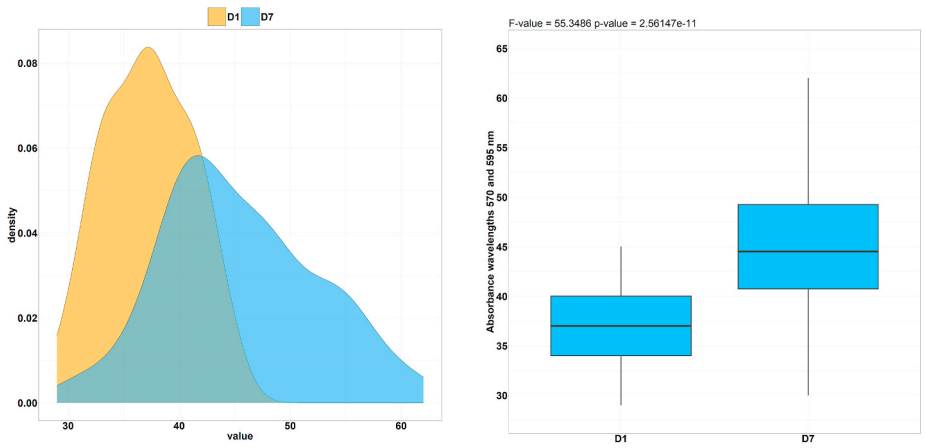

Fig. 7. Results of ANOVA analysis: a) distribution in groups D1 and D7; b) results of dispersion analysis for D1 and D7.

checked using the Shapiro-Wilk test, where results of every group follow a normal distribution (p-value (D1) = 0.4047798 and (D2) = 0.4719734).

Bartlett's test of homogeneity of variances shows that the p-value is $8.652 \cdot 10^{-5}$. So, dispersity is non-homogenous. That is why the dispersed analysis was proved by the Kruskal-Wallis rank-sum test, according to which the p-value is $3.021 \cdot 10^{-10}$, so the valuable difference is existed. Results of ANOVA analysis show F = 55.35, p = $2.56 \cdot 10^{-11}$. Checking normality of residual distribution was provided by the Shapiro-Wilk test, which proved normal distribution (p-value is 0.5658). ANOVA analysis shows a valuable difference between D1 and D7 (P = $2.56 \cdot 10^{-11}$). This conclusion was proved by the Kruskal-Wallis rank-sum test. (p-value = $3.021 \cdot 10^{-10}$).

Collagen production assay can significantly assess cell activity during the proliferation period, and we can confirm low collagen production both in untreated (polished) and polished-HA surfaces in comparison with the sandblasted-HA ones (Fig. 8).

Sample 6 shown significantly less production of collagen within two weeks cultivation compare to the other HA-treated surface. However, Sirius Red absorbance level is still higher comparing the control (NT and #9). It is well known that collagen production is a critical factor for successful implant integration [32], and both surface topography and chemical patterns should influence osteoblast cell adhesion and activity [33]. Increasing average roughness has been shown (both in-vitro and in-vivo) that surfaces with higher Ra have higher rates of osteointegration [34,35]. Additionally, chemical modification, including calcium phosphate (CaP) or HA, is highly osteoconductive and have shown osteointegrative potential in vivo [36,37]. Finally, both strategies (e.g., surface roughness and bioactive coatings) can be combined to achieve synergistic effects. But the best combination strategies and role of each factor in osteointegration are still under discussion. Our data suggest that roughness plays an important role in cell adhesion and proliferation, but HA coating provides additional stimuli for cell activity (collagen synthesis).

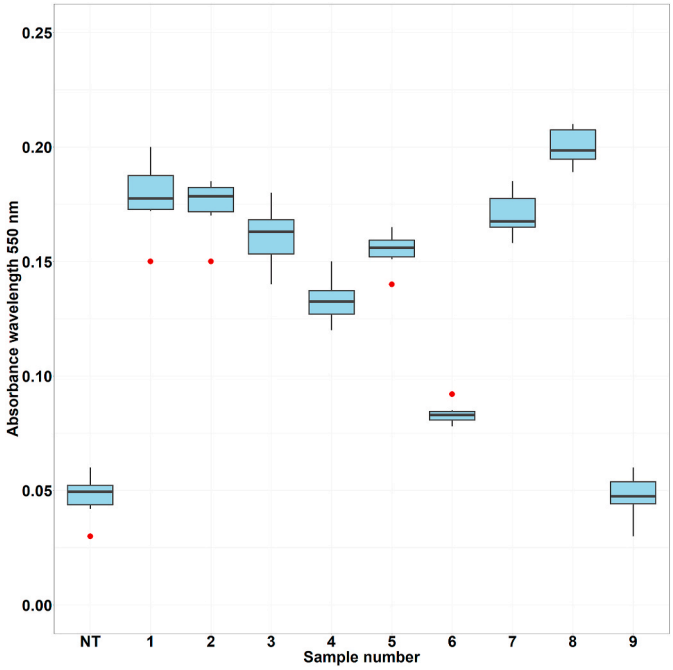

Fig. 8. Sirius Red absorbance level in 14 days after U2OS cell seeding. (For interpretation of the references to color in this figure legend, the reader is referred to the Web version of this article.)

3. Conclusions

In this work, we propose HA coatings deposition from an aqueous electrolyte containing a suspension of nano dispersed hydroxyapatite onto commercially Ti-6Al-4V alloy samples (Grade 4) that were pre-treated by sandblasting combined with different ways (20% NaOH, 20% oxalic acid and combination of 20% oxalic acid and 20% NaOH).

All samples after sandblasting had a rough surface, but HA coatings on the samples without pre-treatment showed higher R_a and R_z values. Roughness plays an essential role in cell adhesion and proliferation, but HA coating provides additional stimuli for cell activity expressed in collagen synthesis. We can confirm low collagen production both in untreated (polished) and polished-HA surfaces in comparison with the sandblasted-HA surfaces. Resazurin reduction assay showed satisfactory U2OS osteoblastic cell adhesion in 1 day of the experiment. There is no significant difference between non-treated polished surfaces and HA-covered with sandblasting pre-treatment. In 7 days, we confirm U2OS cell proliferation on polished Ti substrate and in most HA-coated ones with no significant difference between groups.

But in most cases, we can conclude that sandblasted surfaces that were pretreated with chemical treatments with deposited HA coatings make them more osteoconductive due to increasing of collagen synthesis. All measured contact angles were lower than 90°, which means the formation of hydrophilic HA surfaces when the fluid will spread over a large area of the surface. The hydrophilicity of obtained coatings made them suitable for biomedical applications in dentistry.

CRediT authorship contribution statement

A. Yanovska: Conceptualization, Investigation, Writing - original

draft, Writing - review & editing. **Ye Husak:** Investigation, Data curation, Writing - original draft. **O. Mishchenko:** Conceptualization, Resources, Project administration. **A. Gudakov:** Validation, Formal analysis. **O. Oleshko:** Investigation, Data curation. **A. Yusupova:** Investigation. **M. Vielikov:** Investigation. **J. Radwan-Pragłowska:** Investigation. **M. Piątkowski:** Writing - original draft, Writing - review & editing. **Ł. Janus:** Investigation. **E. Szajna:** Conceptualization, Resources. **M. Pogorielov:** Conceptualization, Methodology, Resources, Writing - review & editing, Supervision, Project administration.

Declaration of competing interest

The authors declare that they have no known competing financial interests or personal relationships that could have appeared to influence the work reported in this paper.

Acknowledgements

This research was funded by EU-H2020-MSCA-RISE, grant no 777926 NanoSurf. The authors acknowledge to grant from Ministry of Education and Science of Ukraine (0119U100823) for support in cell culture research.

References

[1] H.J. Rack, J.I. Qazi, Titanium alloys for biomedical applications, J. Mater. Sci. Eng. C. 26 (2006) 1269–1277, https://doi.org/10.1016/j.msec.2005.08.032.
[2] M.A. Faghihi-Sani, A. Arbabi, A. Mehdinezhad-Roshan, Crystallization of hydroxyapatite during hydrothermal treatment on amorphous calcium phosphate layer coated by PEO technique, J. Ceram. Int. 39 (2013) 1793–1798, https://doi.org/10.1016/j.ceramint.2012.08.026.
[3] The challenge and promise of low-temperature bioceramic coatings, in: R. B. Heimann, J. Surf. Coat. Techn 301 (2016) 1–5, https://doi.org/10.1016/j.surfcoat.2015.12.082.
[4] S. Ferraris, S. Yamaguchi, N. Barbani, M. Cazzola, C. Cristallini, M. Miola, E. Vernè, S. Spriano, Bioactive materials: in vitro investigation of different mechanisms of hydroxyapatite precipitation, J. Acta Biomaterialia 102 (2020) 468–480, https://doi.org/10.1016/j.actbio.2019.11.024.
[5] G. Singh, N. Sharma, D. Kumar, H. Hegab, Design, development and tribological characterization of Ti–6Al–4V/hydroxyapatite composite for bio-implant applications, J. Mat. Chem. Phys. V. 243 (2020), 122662, https://doi.org/10.1016/j.matchemphys.2020.122662.
[6] J.A. Epinette, A. Toni, in: G. Willmann (Ed.), Bioceramics in Joint Arthroplasty, Georg Thieme, Stuttgart, New York, 2001, pp. 84–91.
[7] N. Creugers, The survival of hydroxyapatite-coated implants is questioned, Evid. Base Dent. 3 (3) (2002) 77–78, https://doi.org/10.1038/sj.ebd.6400129.
[8] C. Domínguez-trujillo, E. Peón, E. Chicardi, H. Pérez, J.A. Rodríguez-ortiz, J. J. Pavón, Sol-gel deposition of hydroxyapatite coatings on porous titanium for biomedical applications, J. Surf. Coat. Technol. 333 (2018) 158–162, https://doi.org/10.1016/j.surfcoat.2017.10.079.
[9] A.A. Ivanova, M.A. Surmeneva, R.A. Surmenev, D. Depla, Structural evolution and growth mechanisms of RF-magnetron sputter-deposited hydroxyapatite thin films on the basis of unified principles, J. Appl. Surf. Sci. 425 (2017) 497–506. https://doi:10.1016/j.apsusc.2017.07.039.
[10] H. Nishikawa, T. Hasegawa, A. Miyake, Y. Tashiro, S. Komasa, Y. Hashimoto, Effect of laser fluence and ambient gas pressure on surface morphology and chemical composition of hydroxyapatite thin films deposited using pulsed laser deposition, J. Appl. Surf. Sci. 427 (2018) 458–463, https://doi.org/10.1016/j.apsusc.2017.08.129.
[11] R. Drevet, N. Ben Jaber, J. Fauré, A. Tara, A. Ben Cheikh Larbi, H. Benhayoune, Electrophoretic deposition (EPD) of nano-hydroxyapatite coatings with improved mechanical properties on prosthetic Ti6Al4V substrates, J. Surf. Coat. Techn. 301 (2016) 94–99, https://doi.org/10.1016/j.surfcoat.2015.12.058.
[12] D.H. He, P. Wang, P. Liu, X.K. Liu, F.C. Ma, X.H. Chen, W. Li, J.D. Du, J. Zhao, HA coating fabricated by electrochemical deposition on modified Ti6Al4V alloy, J. Surf. Coat. Technol. 301 (2016) 6–12, https://doi.org/10.1016/j.surfcoat.2015.12.082.
[13] H. Huang, P.-H. Lan, Y.-Q. Zhang, X.-K. Li, Xing Zhang, C.-F. Yuan, X.-B. Zheng, Z. Guo, Surface characterization and in vivo performance of plasma-sprayed hydroxyapatite-coated porous Ti6Al4V implants generated by electron beam melting, J. Surf. Coat. Technol. 283 (2015) 80–88.
[14] T.J. Levingstone, M. Ardhaoui, K. Benyounis, L. Looney, J.T. Stokes, Plasma sprayed hydroxyapatite coatings: understanding process relationships using design of experiment analysis, J. Surf. Coat. Technol. 283 (2015) 29–36.
[15] B.L. Pereira, G. Beilner, C.M. Lepienski, E.S. Szameitat, B.S. Chee, N.K. Kuromoto, L. Luis dos Santos, I. Mazzaro, A.P.R. Alves Claro, M.J.D. Nugent, Oxide coating containing apatite formed on Ti-25Nb-25Ta alloy treated by Two-Step Plasma Electrolytic Oxidation, J. Surf. Coat. Technol. 382 (2020) 125224, https://doi.org/10.1016/j.surfcoat.2019.125224.
[16] S. Lederer, S. Sankaran, T. Smith, W. Fürbeth, Formation of bioactive hydroxyapatite-containing titania coatings on CP-Ti4+ alloy generated by plasma electrolytic oxidation, J. Surf. Coat. Technol. 363 (2019) 66–74, https://doi.org/10.1016/j.surfcoat.2019.02.030.
[17] B. Leandro, A. Rossetto, C. Maurício, I. Mazzaro, N. Kazue, Niobium treated by Plasma Electrolytic Oxidation with calcium and phosphorus electrolytes, J. Mech. Behav. Biomed. Mater. 77 (2018) 347–352, https://doi.org/10.1016/j.jmbbm.2017.08.010.
[18] M.-G. Park, H.-C. Choe, Corrosion behaviors of bioactive element coatings on PEO-treated Ti-6Al-4V alloys, J. Surf. Coat. Technol. 376 (2019) 44–51, https://doi.org/10.1016/j.surfcoat.2018.07.093.
[19] M. Mohedano, X. Lu, E. Matykina, C. Blawert, R. Arrabal, M.L. Zheludkevich, Plasma electrolytic oxidation (PEO) of metals and alloys, in: K. Wandelt (Ed.), Encyclopedia of Interfacial Chemistry, Elsevier, Oxford, 2018, pp. 423–438, https://doi.org/10.1016/B978-0-12-409547-2.13398-0.
[20] A. Santos-Coquillat, M. Mohedano, E. Martinez-Campos, R. Arrabal, A. Pardo, E. Matykina, Bioactive multi-elemental PEO-coatings on titanium for dental implant applications, J. Mater. Sci. Eng. C 97 (2019) 738–752, https://doi.org/10.1016/j.msec.2018.12.097.
[21] A. Yanovska, S. Danilchenko, L. Sukhodub, Fabrication of Nanocomposite Calcium-Phosphate Coatings by Thermal Substrate Method. «Comprehensive Guide for Nanocoatings Technology. Application and Commercialization», vol. 4, Nova Science Publishers, USA. New-York, 2015, pp. 157–183. ISBN: 978-1-63482-648-8.
[22] A. Yanovska, V. Kuznetsov, A. Stanislavov, S. Danilchenko, L. Sukhodub, Synthesis and characterization of hydroxyapatite-based coatings for medical implants obtained on chemically modified Ti6Al4V substrates, Surf. Coating. Technol. 205 (2011) 5324–5329, https://doi.org/10.1016/j.surfcoat.2011.05.040.
[23] L. Zheng, Z. Wu, Y. Zhang, Y. Wei Jun Wang, Effect of non-solvent additives on the morphology, pore structure, and direct contact membrane distillation performance of PVDF-CTFE hydrophobic membranes, J. Environ. Sci. 45 (2016) 28–39, https://doi.org/10.1016/j.jes.2015.09.023.
[24] G. Strnad, N. Chirila, C. Petrovan, O. Russu, Contact angle measurement on medical implant Titanium-based biomaterials, Procedia Technol. 22 (2016) 946–953, https://doi.org/10.1016/j.protcy.2016.01.094.
[25] Y. Yuan, Lee T. Randall, Contact angle and wetting properties, in: G. Bracco, B. Holst (Eds.), Surface Science Techniques, Springer Series in Surface Sciences 51, Springer-Verlag Berlin Heidelberg, 2013, pp. 1–34. ISBN 978-3-642-34242-4.
[26] B. Bhushan, in: B. Bhushan (Ed.), Modern Tribology Handbook, Two Volume Set, first ed., CRC Press, 2000, p. 1760, https://doi.org/10.1201/9780849377877. ISBN 9780849384035.
[27] EN ISO 4287, Geometrical Product Specifications (GPS)—surface Texture: Profile Method—Terms, Definitions, and Surface Texture Parameters, International Organization for Standardization, Geneva, 1999. ISO, 1997. - 36 pp.
[28] DIN 4768, Determination of Values of Surface Roughness Parameters Ra, Rz, Rmax Using Electrical Contact (Stylus) Instruments; Concepts and Measuring Conditions, Deutsches Institut fur Normung E.V. (DIN), 1990, p. 3. Published by.
[29] T.H. Huang, C.C. Yang, S.J. Ding, M. Yan, M.Y. Chou, C.T. Kao, Biocompatibility of human osteosarcoma cells to root end filling materials, J. Biomed. Mater. Res. B Appl. Biomater. 72B (2005) 140–145, https://doi.org/10.1002/jbm.b.30137.
[30] A. Yanovska, V. Kuznetsov, A. Stanislavov, E. Husak, M. Pogorielov, V. Starikov, S. Bolshanina, S. Danilchenko, Synthesis and characterization of hydroxyapatite-gelatine composite materials for orthopedic application, J. Mat. Chem. Phys. 183 (2016) 93–100, https://doi.org/10.1016/j.matchemphys.2016.08.006.
[31] S.-L. Bee, M. Mariatti, N. Ahmad, B.H. Yahaya, Z.A. Abdul Hamid, Bio-CAM 2017 Effect of the calcination temperature on the properties of natural hydroxyapatite derived from chicken bone wastes, Mater. Today: Proc. 16 (2019) 1876–1885, https://doi.org/10.1016/j.matpr.2019.06.064.
[32] S. Huang, A. Ulloa, E. Nauman, L. Stanciu, Collagen coating effects on Fe-Mn bioresorbable alloys, J. Orthop. Res. 38 (3) (2020) 523–535, https://doi.org/10.1002/jor.24492.
[33] H.F. Pereira, I.F. Cengiz, F.S. Silva, R.L. Reis, J.M. Oliveira, Scaffolds and coatings for bone regeneration, J. Mater. Sci. Mater. Med. 31 (3) (2020) 27, https://doi.org/10.1007/s10856-020-06364-y.
[34] J. Tavakoli, M.E. Khosroshahi, Surface morphology characterization of laser-induced titanium implants: lesson to enhance osseointegration process, Biomed. Eng. Lett. 8 (3) (2018) 249–257, https://doi.org/10.1007/s13534-018-0063-6.
[35] I. Gnilitskyi, M. Pogorielov, R. Viter, et al., Cell and tissue response to nanotextured Ti6Al4V and Zr implants using high-speed femtosecond laser-induced periodic surface structures, J. Nanomed.: Nanotechnol. Biol. Med. 21 (2019), 02036, https://doi.org/10.1016/j.nano.2019.102036.
[36] S. Burtscher, P. Krieg, A. Killinger, A. Al-Ahmad, M. Seidenstücker, S.H. Latorre, A. Bernstein, Thin degradable coatings for optimization of osteointegration associated with simultaneous infection prophylaxis, Materials 12 (21) (2019) 25, https://doi.org/10.3390/ma12213495.
[37] Y. Su, I. Cockerill, Y. Zheng, L. Tang, Y.X. Qin, D. Zhu, Biofunctionalization of metallic implants by calcium phosphate coatings, J. Bioact. Mater. 4 (2019) 196–206, https://doi.org/10.1016/j.bioactmat.2019.05.001.